

# Computational Modeling of Geosynthetic Reinforced Soil (GRS) Composites Under Axial Loading

Marta Sitek<sup>1</sup>  
Cezary Bojanowski<sup>1</sup>

1) Transportation Research and Analysis Computing Center  
Energy System Division  
Argonne National Laboratory  
9700 S. Cass Avenue  
Argonne, IL 60439-4828, USA  
[msitek@anl.gov](mailto:msitek@anl.gov), [cbojanowski@anl.gov](mailto:cbojanowski@anl.gov)

## Abstract

*Modeling the behavior of a granular medium, such as soil, as a finite element continuum is a challenging task. A significant number of constitutive models for soils are implemented in commercial software, but their application is limited to specific cases. The main goal of the work presented in this paper was to select a soil model implemented in LS-DYNA<sup>®</sup> that performs best in simulating a laboratory compression test of geosynthetic reinforced soil (GRS).*

*The full-scale geosynthetic reinforced soil composite tests were performed at FHWA's Turner-Fairbank Highway Research Center. An example of a free-standing mini-pier test in a three-dimensional stress-strain state is considered. The specimens vary with geosynthetic reinforcement strength and spacing. The models are built in stages, as soil is placed layer by layer, with geotextile inserts, and compacted. The specimens are then axially loaded until collapse. The history of vertical displacements of the top surface, horizontal displacements on the free surfaces and the ultimate load are recorded and compared with the experimental results.*

*A preliminary study was performed to find the most appropriate soil material model available in LS-DYNA, which would represent well the behavior of granular soil in interaction with a geotextile. Computational results closest to experimental ones were obtained with the use of the \*MAT\_HYSTERETIC\_SOIL (079) model in combination with the \*MAT\_FABRIC (034) material model to represent the behavior of the geotextile. Additionally, the model \*MAT\_ADD\_EROSION was used to simulate the failure of the geosynthetic material under loading.*

*The simulations show a good correspondence with the experiments. Failure modes of the computational models are similar to the ones obtained in the laboratory. Even though local damage of the soil was not captured, the axial strain and the failure load are represented well.*

**Keywords:** geosynthetic reinforced soil, soil-geotextile interaction, soil modeling

### 1. Introduction

Geosynthetic reinforcement has many applications in geotechnical structures. One of the most common among them is reinforcing the bridge embankments at abutments. The geosynthetic reinforcement improves stability and reduces deformations thus allowing higher embankments with steeper slopes to be built.

Full-scale Geosynthetic Reinforced Soil (GRS) tests with a free-standing Mini Pier [1], were performed at FHWA’s Turner-Fairbank Highway Research Center with the goal of establishing the influence of the reinforcement’s spacing and its strength on failure modes and critical load for the composites. The goal of the research presented here was to assess the possibility of computational modeling of these laboratory experiments on GRS specimens in LS-DYNA. First, a preliminary research was performed to establish the best suitable soil material model available in the software. Results of triaxial tests performed in the laboratory environment were used as a reference. Second, the chosen model with calibrated material properties was used to represent the backfill in the GRS tests.

### 2. Investigation of Material Models for Backfill Modeling

The backfill used in all tests was AASHTO A-1-a aggregate (see [2] for AASHTO soil classification). In the first stage of the research the results of triaxial compression tests found in report [3] were used to perform a comparative study of selected material models available in LS-DYNA. The results covered deviatoric stress vs. volumetric strain curves for a set of confining pressures: 5, 10, 30, 70 and 100 psi. Figure 1 shows stress vs. strain curves obtained in these experiments. The main characteristics of these plots is varying initial slope for all the curves resulting from dependency of most soil properties on the pressure. This feature was of interest for the numerical study.

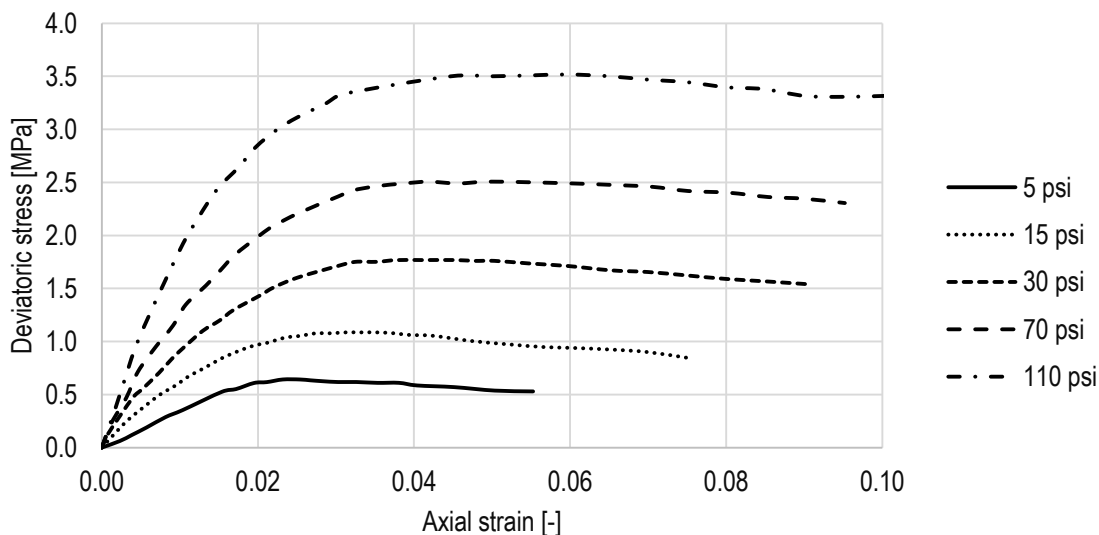


Figure 1: Experimental triaxial compression test results for various levels of confining pressure

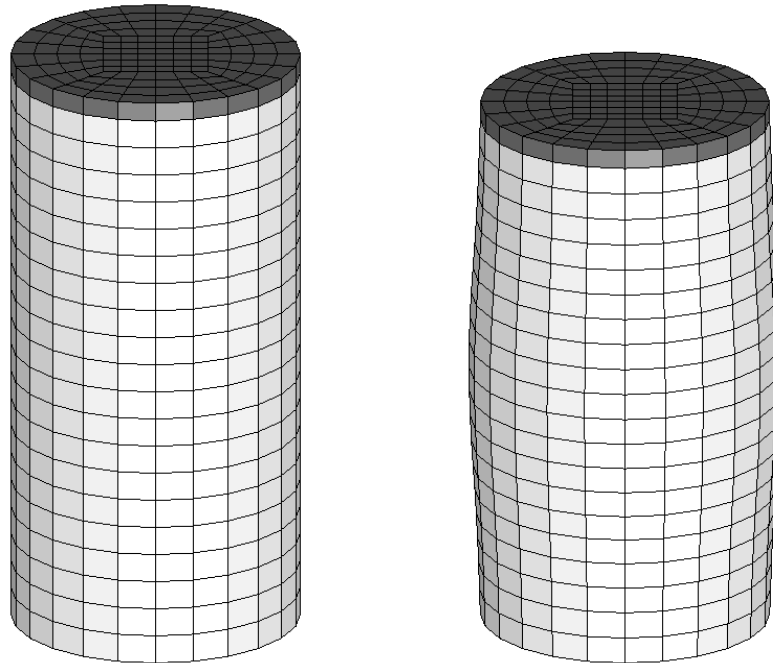


Figure 2: Finite Element model of the soil sample for triaxial test simulations

LS-DYNA contains a large library of constitutive models that can be used for simulating geomaterials (such as: soil, concrete and rock). Models: MAT\_005 (Soil and Foam), MAT\_025 (Geologic Cap), MAT\_079 (Hysteretic Soil), and MAT\_193 (Drucker-Prager) were tested in simulations of the triaxial compression test. Each of them has a significantly different formulation and most of them require many more material parameters than the typically used geotechnical constants (as cohesion, angle of internal friction or angle of dilation).

Figure 2 presents the geometry and the mesh of the triaxial test sample model before and after deformation. The model represents a cylindrical sample with dimensions 0.315 m in height and 0.152 m in diameter. A rigid plate was modeled on the top and a uniform pressure was applied to it. The translational degrees of freedom of the bottom nodes were constrained.

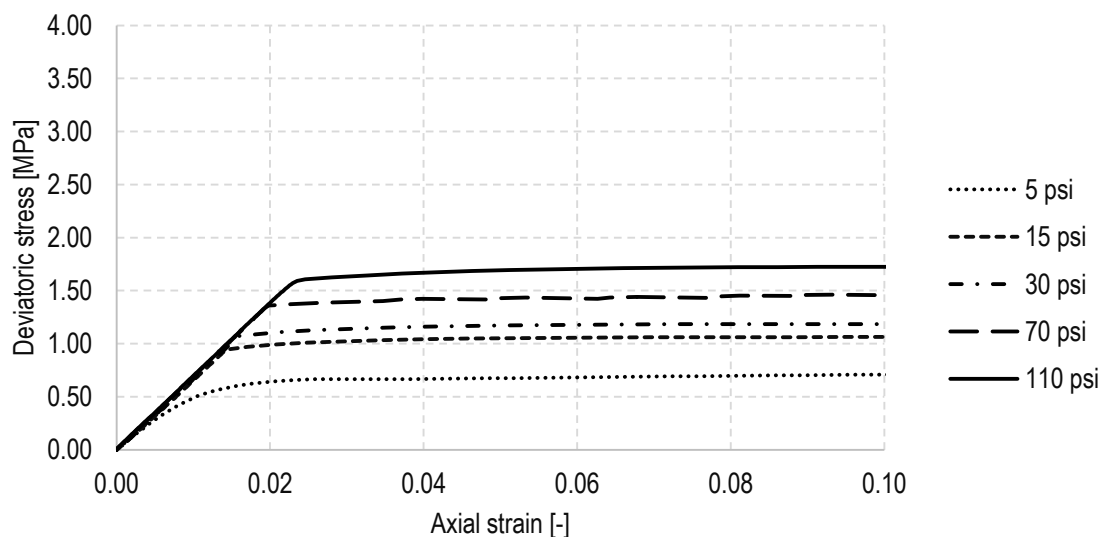


Figure 3: Triaxial test results for material model MAT\_005

Figure 3 shows triaxial test results for MAT\_005 (SOIL AND FOAM) model. The deviatoric stress-strain curves are linear in the elastic range and almost perfectly plastic outside of it. Only for the lowest confining pressure was the transition smoother and the curve more pronounced. The sample strength (deviatoric stress) was significantly underpredicted for all the cases making this model not suitable for further study.

A material model developed by FHWA, MAT\_FHWA\_SOIL (MAT\_147) is an isotropic model with damage. When used to model a triaxial test, it doesn't capture the material stiffness dependence on the stress state, therefore the initial slope is the same for all confining pressures, see Figure 4. Moreover, there is no noticeable limit on the stresses which should occur with the increase of strains. Instead, the gradients increase with increasing plate displacement for lower confining pressures. This material model was also excluded from further analysis.

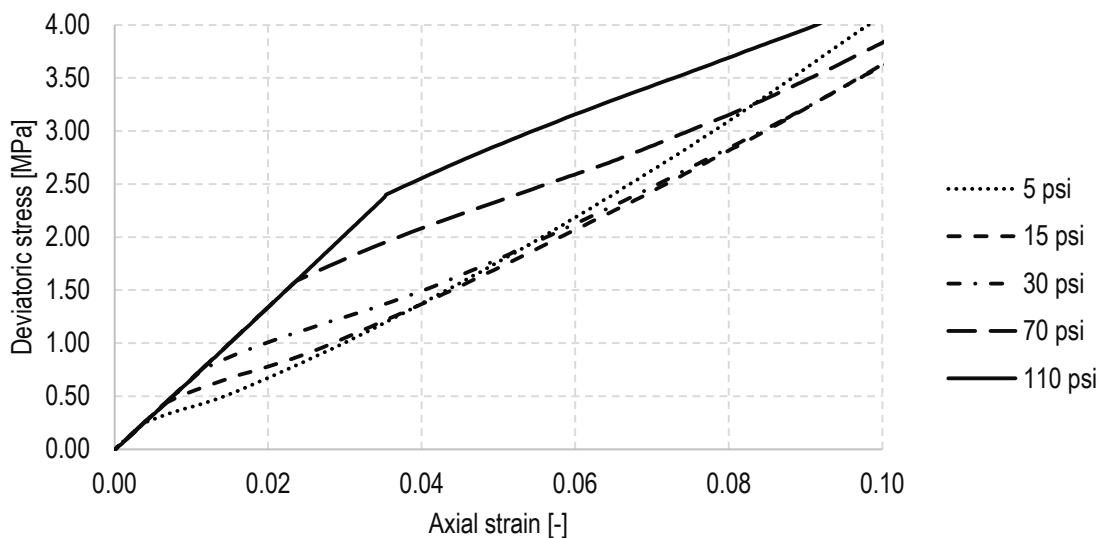


Figure 4: Triaxial test results for material model MAT\_147

Figure 5 shows curves of axial strain vs. vertical stress for material model MAT\_193 (Drucker-Prager). The Drucker-Prager model is a simple material model which also does not have the ability to simulate pressure-dependent moduli. The model was not able to capture the failure load accurately as well. The stresses in the model were increasing without reaching an expected plateau, thus, this model was not investigated further.

Figure 6 presents the results of triaxial compression tests with MAT\_025 (Geologic cap). This model was able to capture the strength of the samples better than the other tested models. The initial slope of the curves is not pressure dependent and the axial strains at failure load are much higher than in the experiment. Therefore it is not able to represent properly the initial behavior of the soil samples and was not used in further computations.

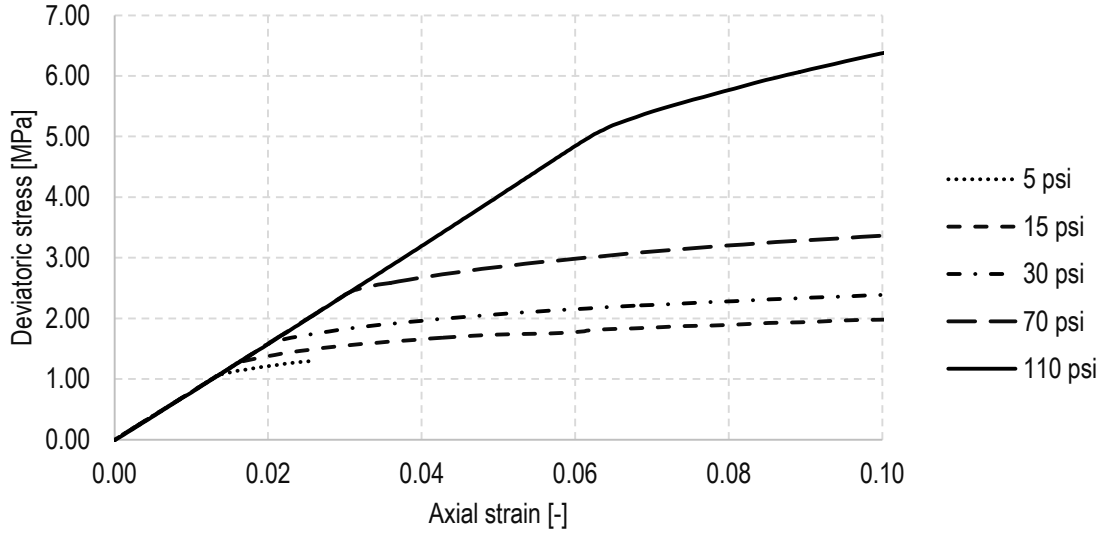


Figure 5: Triaxial compression simulation results for MAT\_193

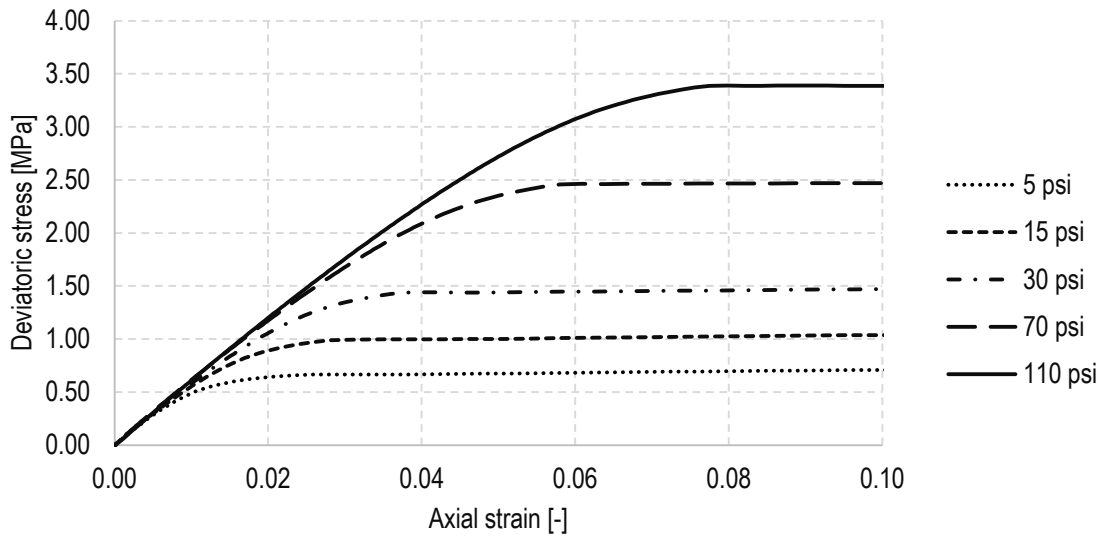


Figure 6: Triaxial compression simulation results for MAT\_025

Hysteretic soil model (MAT\_079) is a nested surface model with up to ten superposed ‘layers’ of elastic-perfectly plastic material, each with its own elastic moduli and yield stress values.

The elastic moduli  $K$  and  $G$  are functions of pressure:

$$K(p) = \frac{K_0(p-p_0)^b}{(p_{ref}-p_0)^b}, \quad G(p) = \frac{G_0(p-p_0)^b}{(p_{ref}-p_0)^b},$$

where  $p$  is the current pressure, calculated as follows

$$p = [-K_0 \ln V]^{\frac{1}{1-b}},$$

where  $V$  - the relative volume is calculated as the ratio between the initial and current volume in a hydrostatic compression test.

Yield function constants,  $a_0$ ,  $a_1$  and  $a_2$ , are calculated as

$$a_0 = \frac{12c^2(\cos \phi)^2}{(3-\sin \phi)^2}, \quad a_1 = \frac{24c \sin \phi \cos \phi}{(3-\sin \phi)^2}, \quad a_2 = \frac{4(\sin \phi)^2}{3(3-\sin \phi)^2},$$

where the values of cohesion,  $c$ , and angle of internal friction,  $\phi$ , are presented in Table 1.

Table 1: Values of yield function constants for different strength parameters

	$\phi$ [deg]	$c$ [MPa]	$a_0$	$a_1$	$a_2$
Triaxial test	50	0.071	0.0050	0.1682	0.1568
Mini-pier test	53	0.055	0.0027	0.1309	0.1755

Reference pressure  $p_{ref}$  is the pressure for which direct shear test results, meaning shear stress vs. shear strain curves, are known and supplied to the model. Laboratory tests were performed for  $p_{ref} = 10, 20$  and  $30$  psi (see Figure 7). The resultant curves are introduced into the model as piecewise linear. Hydrostatic test results are used to establish the bulk modulus  $K_0$  at the reference pressure as a secant modulus of mean stress – volumetric strain curves in the vicinity of  $p_{ref}$ .

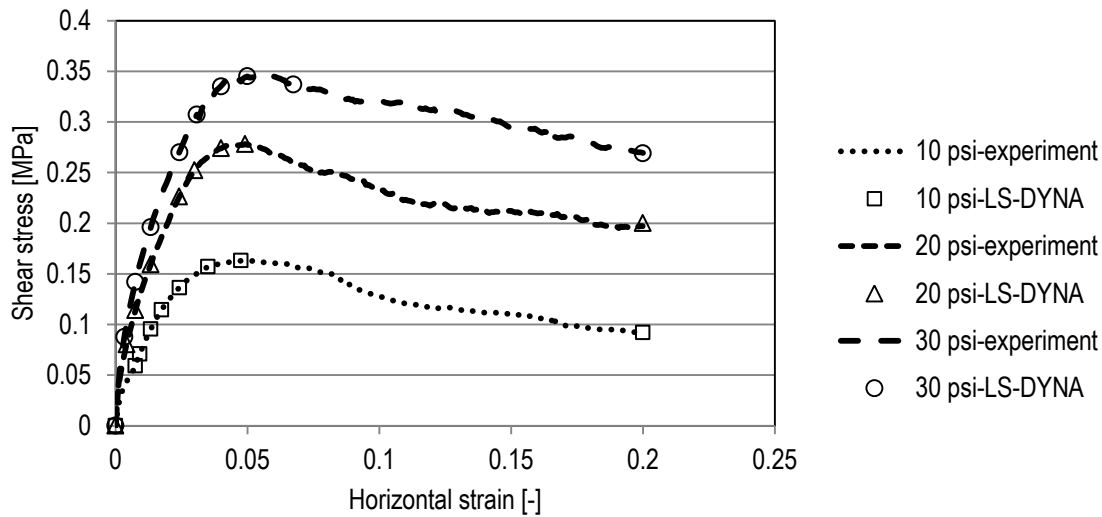


Figure 7: Experimental shear stress - shear strain curves and the approximation

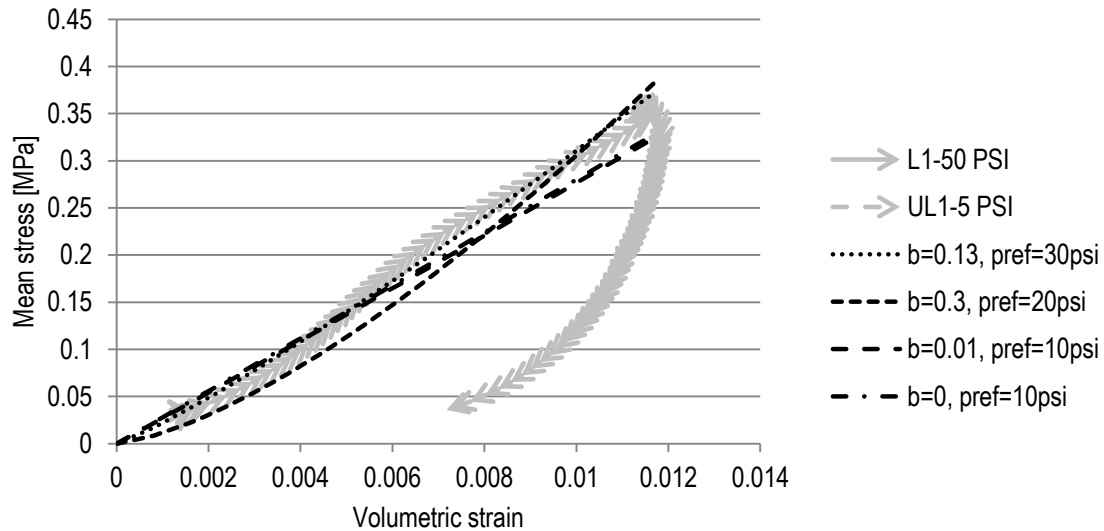


Figure 8: First loading-unloading cycle of a hydrostatic test and four example curves calculated for various input parameters

Figure 8 shows the first loading-unloading cycle of the performed hydrostatic test and the best fit curves obtained for  $p_{ref} = 10, 20$  and  $30$  psi with (1)  $b > 0$  and (2)  $b = 0$ . The first loading curve was used to calculate the bulk modulus  $K_0$  at the reference pressure levels. The corresponding values are presented in Table 2.

Table 2: Reference pressures and corresponding bulk moduli

$p_{ref}$	$K_0$ [MPa]
10 psi (0.07 MPa)	28
20 psi (0.138MPa)	43
30 psi (0.207MPa)	36

MAT\_079 model allows for pressure dependence in the soil elastic properties. Thanks to this feature, the initial slope of the stress – strain curves varies for the selected confining pressures (see Figure 9). This model requires more input data than the previously checked models, which can be obtained from additional tests, such as: triaxial compression test, hydrostatic compression test and direct shear test (shear stress vs. strain curve is necessary). Moreover, the stresses reach a plateau and approximate the failure stress quite well. This model was used in further studies, as it gave the most accurate results.

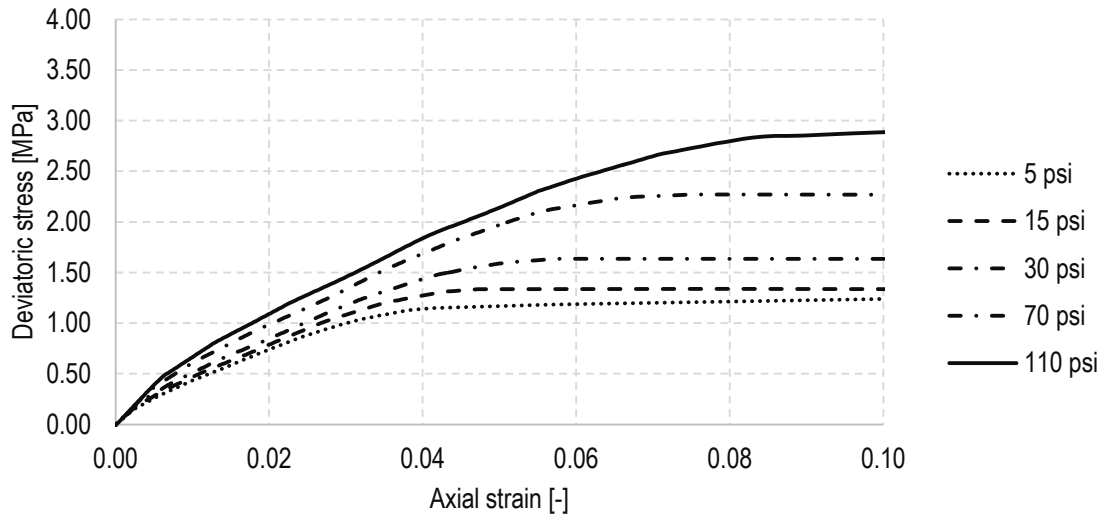


Figure 9: Triaxial compression simulation results for MAT\_079

After a consultation with the material model developers, we learned that this material model was developed mainly for seismic response and soil-structure interaction applications. The use of exponent  $b$  greater than zero can cause issues and ‘it makes the response noisy’. Instead, it was recommended to apply different material properties to horizontal layers of soil, corresponding to its initial stress state. This approach requires the following procedure:

- apply gravity loading to the sample and record the pressure values in a few layers,
- calculate  $K(p) = \frac{K_0(p-p_0)^b}{(p_{ref}-p_0)^b}$  with appropriate choice of  $b$  for those layers,
- use the resulting  $K_0$ , set  $b$  to zero and  $a_0, a_1, a_2$  as calculated earlier.

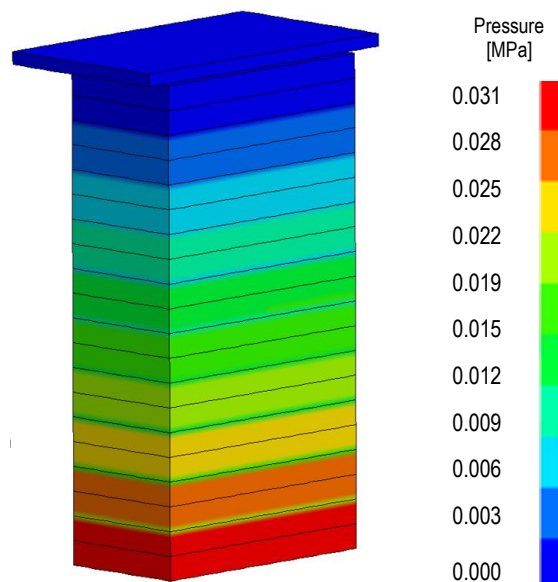


Figure 10: Pressure levels resulting from gravity loading in a TF-7 test model

Figure 10 shows an example of a cross-section through a GRS TF-7 sample with pressure levels resulting from gravity loading. All pressure values fall under 0.03 MPa. For this pressure level,

the bulk modulus calculated for  $p_{ref} = 10$  psi is very close to the initial value of 28 MPa, therefore this value will be adopted.

### 3. Geosynthetic Reinforcement Modeling

In the laboratory experiments, the backfill was reinforced with geotextile Geotex 4x4, its properties are described in [4]. Two cases of reinforcement were considered: single sheet and double sheet of the geosynthetic. Load-deformation curves for both cases, as established in tests [3], are shown in Figure 11.

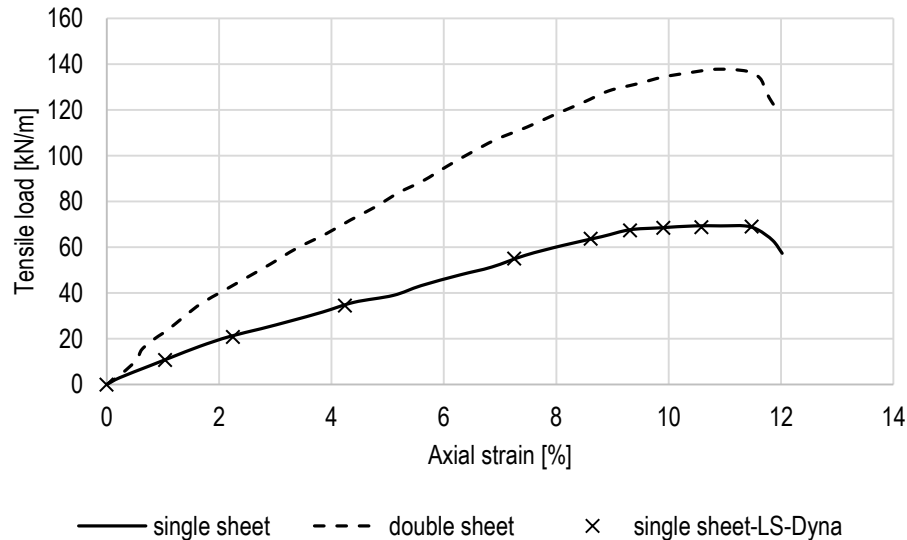


Figure 11: Stress-strain curves for one and two sheets of Geotex 4x4, obtained from a tensile test and the curve applied in \*MAT\_FABRIC material model

Material model \*MAT\_FABRIC (MAT\_034) was chosen to represent the behavior of the geosynthetic. This model allows orthotropic elastic characteristics of thin fabrics modeled as membranes to be defined. The stress - strain relationship can be defined in piecewise linear form on the basis of the curves obtained in an experiment for a single sheet. In the report [3] it was stated that Geotex 4x4 behaves like an isotropic material and therefore the same curve applies to both directions. The material density of this material equals  $2500 \text{ kg/m}^3$  and Poisson's ratio is 0.2. This model doesn't take into account plastic behavior or failure of the material. An additional keyword was used, \*MAT\_ADD\_EROSION, to simulate the failure of the geosynthetic under loading. Tests showed that it breaks at approximately 10% of axial strain, therefore a strain failure criterion was used, with effective strain at failure (EFFEPS) equal 0.1. When the criterion is met in the simulation, the finite element is deleted from further computations.

### 4. Mesh Density Study

A mesh density study was performed for GRS model tests on the basis of a TF-7 sample. Three mesh densities were considered, coarse, medium and dense, with finite elements sizes decreasing 2:1, which gave 3500, 28000 and 216000 finite elements respectively. The resulting FEM discretizations are presented in Figure 12. The finest mesh was selected for further computations. The failure mode in that simulation resembled the failure in the experiment.

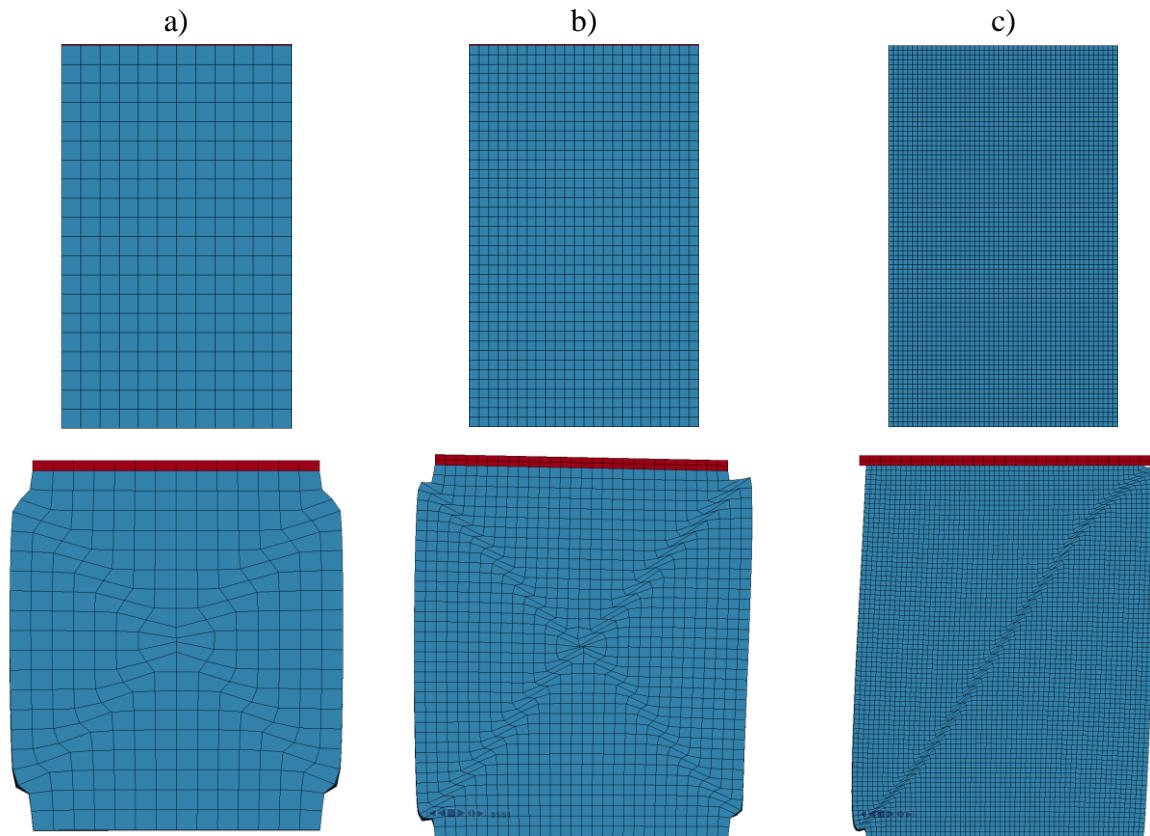


Figure 12: Discretization of the soil sample model.

### 5. Modeling of the Construction Process of a GRS Sample

Three test cases were chosen from report [1] as a reference to study the robustness of soil modeling in LS-DYNA. Table 3 presents the test setup, with the basic properties of backfill used, reinforcement stiffness, and spacing.

Table 3: Mini pier tests setup

Test nr	Backfill	Reinforcement	
		Stiffness [lb/ft]	Spacing [in]
TF-3	Type: 21A, $\phi=50^\circ$ , c=0.55 MPa	2400	$7 \frac{5}{8}$
TF-7		4800	$7 \frac{5}{8}$
TF-10		4800	$15 \frac{1}{4}$

The construction stages of the specimen were as follows:

- Place the first layer of cement blocks and first soil layer and apply compaction load.
- Place 2<sup>nd</sup> soil layer and apply compaction.
- Place 1<sup>st</sup> geogrid on top of the layer of soil,
- Repeat previous steps until the last layer of soil is added and compacted.
- Remove the blocks forming walls, trim the excess of the reinforcement.

- Apply vertical displacement to the top of the specimen through a rigid plate, until failure.

In the simulation the construction process was divided into steps. The loads are applied incrementally from zero to full value in the first half of each step. To model the construction stages, gravity load of the parts was added at different times in the simulation. The samples are 1m by 1m by 2m. Compaction was performed on each of 0.1 m soil layers with a distributed surface load of 52 kPa. The gravity loads were kept constant throughout the simulation and the compaction loads decreased to zero at the end of a step. These functions change values from 0 to 1 and are multiplied by an appropriate value of gravity acceleration or compaction load. Additional models were built for tests TF-3 and TF-7 (see Figure 14 and Figure 15) in which gravity loading was applied to all parts at once and compaction load was omitted. This approach saves computational time and resources, but the results differ from those obtained in the more complex model. Contrarily to the expected outcome, the specimen is stiffer, giving a higher failure load and lower vertical strain.

The backfill as well as loading plate were modeled with 8-node solid finite elements (ELFORM=1). The reinforcement was modeled with 4-node shell finite elements (ELFORM=9). The backfill was modeled with ~136,000 solid hexagonal elements and the geogrid with ~15,000 quadrilateral shell elements. There was no interface (or contact) defined between the soil and reinforcement, instead, the adjacent finite elements share the same nodes.

The only separate part was a rigid loading plate, which at the beginning of the simulation was positioned above the sample. Horizontal displacements of the plate were constrained, so that only vertical movement was possible. Prescribed vertical downward displacement was applied to the plate. This displacement was kept at zero during the first seconds of the simulation, until the gravity and compaction loads were fully applied and the vertical displacements in the specimen stabilized.

Contact between the plate and top soil layer was modeled with the use of \*AUTOMATIC NODES TO SURFACE with a soft constraint option and static and dynamic friction coefficients equal to 0.7. To simplify the model, the concrete blocks were represented by constraints on the horizontal displacements on the walls of the specimen. The horizontal displacements were fixed on the vertical walls throughout the building process, then the constraints were removed.

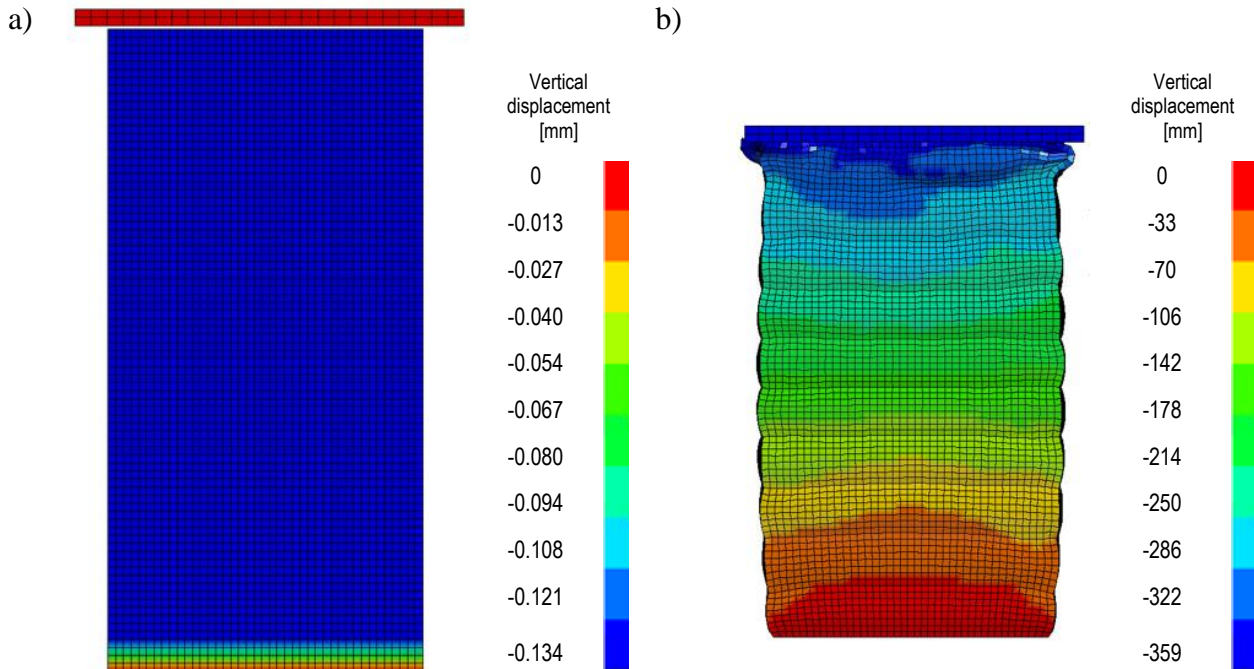


Figure 13: Test TF-7. Vertical displacement contour plots a) at the first and construction stage and b) at failure load

## 6. Validation of the Model

The model was pre-loaded in stages as was done in the real test. Figure 13 (a) shows the vertical displacement field in the model at the end of the first construction phase. The entire geometry of the domain is present in the model from the beginning, but the layers are ‘activated’ one by one, by applying appropriate gravity loads. Therefore, in the first stage only the vertical displacements of the first layer vary, for the rest of the sample the displacements are constant and equal to the highest displacement on top of the first layer. Figure 13 (b) shows the deformation of the sample at the failure load.

Axial load vs. axial strain graphs for the considered mini-pier tests, TF-3, TF-7 and TF-10, are presented in Figure 14, Figure 15, and Figure 16 respectively. Computational results are compared with the experimental outcome. Tests TF-3 and TF-7 gave results close to the experimental value for the chosen material parameters and finite element mesh. The simulations with bulk modulus dependent on pressure ( $b=0.01$ ) were very close to the experimental value estimation of the failure load. The maximum vertical load in test TF-3 is 864 kPa with 13.7% axial strain, compared to an experimental value 838 kPa at 13.8% strain. Test TF-7 gives 1199 kPa failure load at 15.8% vertical strain as compared to 1273 kPa at 16% strain. The computations with  $b=0$  give a very similar initial slope of the curve with failure load higher than expected. The computational failure load for test TF-3 was 960 kPa with axial strains of 13.6%. Results of test TF-7 were 1566 kPa at 17%. The model of the test TF-10 gave an overly stiff response for the same numerical setup. Axial strains at failure were very similar, 14.8% in the model and 14.3% in the experiment. In this case, the reinforcement is spaced more sparsely and therefore the deformation of soil has more influence on the overall behavior of the sample.

Material model MAT\_025 was also tested in GRS simulations, as it gave good results in modeling the triaxial test. Different values of the input parameters were applied, but none of them performed well: the response was overly stiff in all cases.

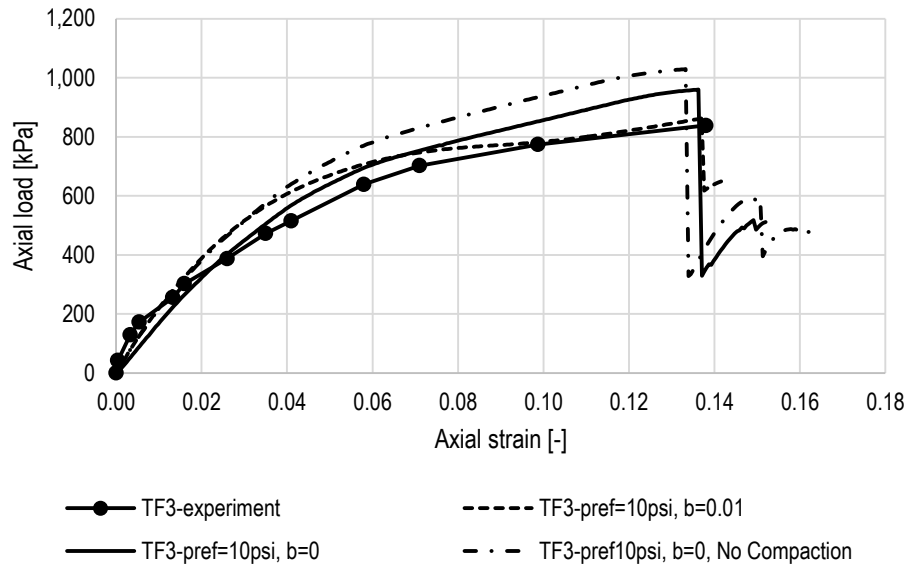


Figure 14: Comparison of experimental and numerical stress - strain dependence of test TF-3

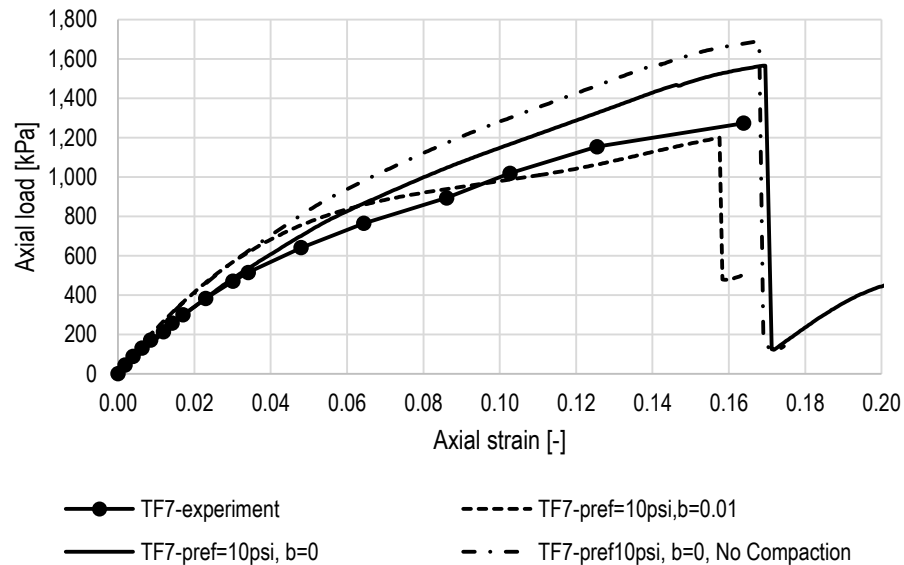


Figure 15: Comparison of experimental and numerical stress - strain dependence of test TF-7

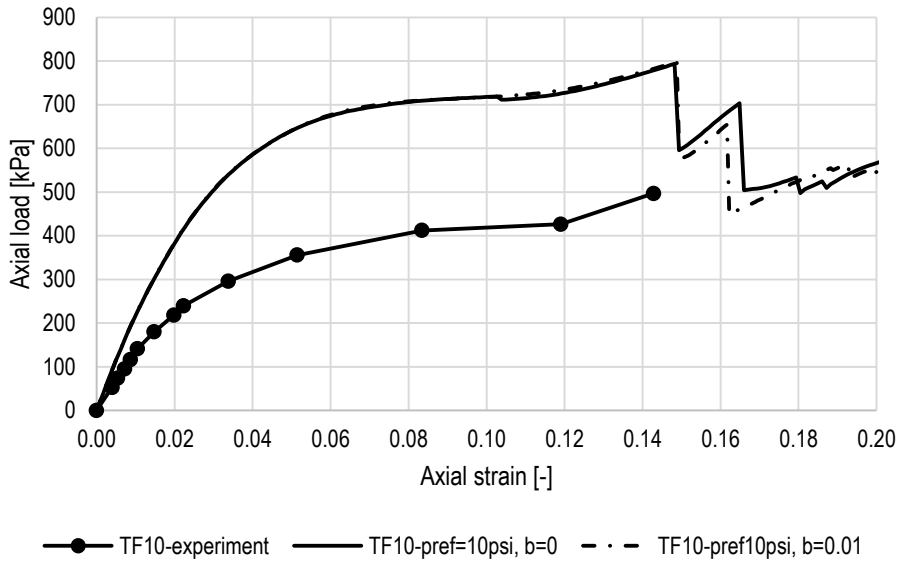


Figure 16: Comparison of experimental and numerical stress - strain dependence of test TF-10

Lateral displacement along the height of GRS samples at two load levels can be found in Figure 17. The report [1] delivers results only for the TF-7 test. A good match between the computational and experimental results was obtained for lower load level. For the failure load the experimental data is limited to four points, as part of the backfill fell off during the laboratory test. The maximum measured horizontal displacement is equal to 59 mm, whereas the numerical value is equal to 45.8 mm. TF-10 results show the highest displacement values compared to all other cases.

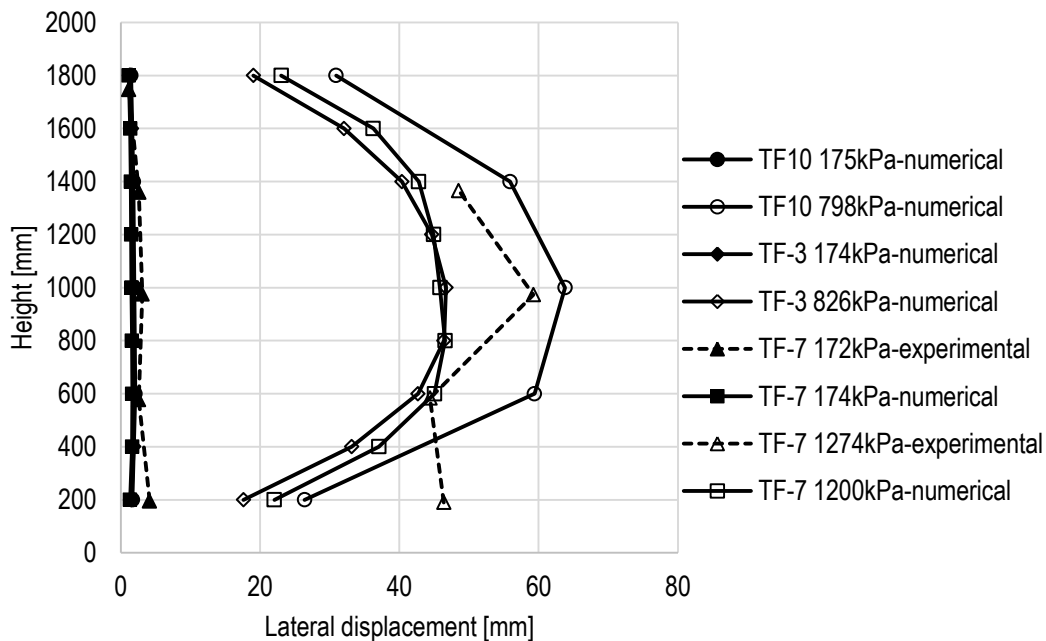


Figure 17: Horizontal displacements of selected points on the specimen walls at approximately 174 kPa axial load and at failure load

## Summary

In the paper, modeling of GRS tests is presented. Different soil material models were considered for use in the computations and their performance was verified on a series of triaxial tests. The computations showed that MAT\_025 and MAT\_079 performed better than the other studied models. They were applied to model backfill in mini-pier georeinforced soil tests. Material model MAT\_025 overestimated stiffness of the samples in every case. In contrast, MAT\_079 gave a good approximation of the axial load vs. axial strain relationships.

Investigation of the results indicates that the accuracy of the results for this model depend on the proportion of backfill to geotextile. The simulations with higher number of reinforcement sheets give results closer to the experimental data, with vertical strain and stress at failure very close to the experimental values. In the case of test TF-10, where there are only four sheets of reinforcement (instead of 9 as compared to the other two tests), the model is significantly stiffer. The reason for this behavior may lie in the type of failure experienced in the test. In the experiment failure begins with a backfill loss from in between the geotextile layers. This decreases the area of the horizontal cross-sections and consequently weakens the specimen early in the loading process. In the model such a deformation was absent.

Overall, the presented approach to modeling GRS structures performed well in the considered examples. Additional research is needed to address the mentioned issues.

## Acknowledgements

Argonne National Laboratory is a U.S. Department of Energy laboratory managed by UChicago Argonne, LLC. Argonne's Transportation Research and Analysis Computing Center (TRACC) is funded by the U.S. Department of Transportation. This research was funded by FHWA Turner-Fairbank Research Center under interagency agreement IAA DTFH61-14-X-300002. The authors acknowledge the strong support from TRACC's Director, Dr. Hubert Ley and proofreading of Dr. Steven Lottes.

## References

- [1] Nicks J.E., Adams M.T., Ooi P.S.K., Stabile T., Geosynthetic Reinforced Soil Performance Testing – Axial Load Deformation relationships, FHWA-HRT-13-066, 2013
- [2] Engineers Daily, AASHTO Soil Classification System, <http://www.engineersdaily.com/2011/03/aashto-soil-classification-system.html>, last accessed 03.03.2016
- [3] Wu J.T.H., Pham T.Q., Adams M.T., Composite Behavior of Geosynthetic Reinforced Soil Mass, FHWA-HRT-10-077, 2013
- [4] <http://geotextile.com/downloads/Geotex%20x4%20Product%20Data%20Sheet.pdf> Propex, <http://propexglobal.com/GeoSolutions/Product-Tour/GEOTEX-Woven> last accessed 03.03.2016

The submitted manuscript has been created by UChicago Argonne, LLC, Operator of Argonne National Laboratory ("Argonne"). Argonne, a U.S. Department of Energy Office of Science laboratory, is operated under Contract No. DE-AC02-06CH11357. The U.S. Government retains for itself, and others acting on its behalf, a paid-up nonexclusive, irrevocable worldwide license in said article to reproduce, prepare derivative works, distribute copies to the public, and perform publicly and display publicly, by or on behalf of the Government. The Department of Energy will provide public access to these results of federally sponsored research in accordance with the DOE Public Access Plan. <http://energy.gov/downloads/doe-public-accessplan>